Complex membrane remodeling during virion assembly of the 30,000 years-old Mollivirus sibericum

E Quemin, S Corroyer-Dulmont, A Baskaran, E Penard, Anastasia Gazi, E Christo-Foroux, P Walther, Chantal Abergel, J Krijnse-Locker

JVI Accepted Manuscript Posted Online 17 April 2019
J. Virol. doi:10.1128/JVI.00388-19

Complex membrane remodeling during virion assembly of the 30,000 years-old Mollivirus sibericum

Quemin ER[a*], Corroyer-Dulmont S[a], Baskaran A[a*], Penard E[a], Gazi AD[a], Christo-Foroux E[b], Walther P[c], Abergel C[b#], Krijnse-Locker J[a#]

[a] Ultrastructural Bio-imaging (UBI), Center for ressources and research in technology (C2RT) and Department of Cell Biology and Infection, Institut Pasteur, 25-28, rue du Dr. Roux, 75015 Paris, France.

[b] Aix-Marseille University, Centre National de la Recherche Scientifique, Information Génomique & Structurale, Unité Mixte de Recherche 7256 (Institut de Microbiologie de la Méditerranée, FR3479), 13288 Marseille Cedex 9, France.

[c] Electron Microscopy (EM) Core Facility, University of Ulm, Ulm, Germany.

Running head: Inner membrane assembly of Mollivirus sibericum

[#]Adress correspondence to Chantal Abergel chantal.Abergel@igs.cnrs-mrs.fr and Jacomina Krijnse-Locker jacomina.krijnse-locker@pasteur.fr

*Present address:

Emmanuelle R. Quemin – Structural Cell Biology of Viruses, Center for Structural Systems Biology, Notkestrasse 85, 22607 Hamburg, Germany.

Asha Baskaran – Institut du Cerveau et de la Moelle Epinière, Hôpital Pitié Salpêtrière, 47, boulevard de l'hôpital, 75013 Paris, France.

Abstract

Cellular membranes ensure functional compartmentalization by dynamic fusion-fission remodeling and are often targeted by viruses during entry, replication, assembly and egress. Nucleocytoplasmic large DNA viruses (NCLDVs) can recruit host-derived open membrane precursors to form their inner viral membrane. Using complementary 3D-electron microscopy techniques including focused-ion beam scanning electron microscopy and electron tomography, we show that the giant Mollivirus sibericum utilizes the same strategy but also displays unique features. Indeed, assembly is specifically triggered by an open cisterna with a flat pole in its center and open curling ends that grow by recruitment of vesicles, never reported for NCLDVs. These vesicles, abundant in the viral factory (VF), are initially closed but open once in close proximity to the open curling ends of the growing viral membrane. The flat pole appears to play a central role during the entire virus assembly process. While additional capsid layers are assembled from it, it also shapes the growing cisterna into immature crescent-like virions and is located opposite to the membrane elongation and closure sites, thereby providing virions with a polarity. In the VF, DNA-associated filaments are abundant and DNA is packed within virions, prior to particle closure. Altogether, our results highlight the complexity of the interaction between giant viruses and their host. Mollivirus assembly relies on the general strategy of vesicle recruitment, opening and shaping by capsid layers similar to all NCLDVs studied until now. However, the specific features of its assembly suggests that the molecular mechanisms for cellular membrane remodeling and persistence are unique.

Importance

Since the first giant virus Mimivirus was identified, other giant representatives are isolated regularly around the World and appear to be unique in several aspects. They belong to at least four viral families and the ways they interact with their hosts remain poorly understood. We focused on Mollivirus sibericum, the sole representative of “Molliviridae” which was isolated from a 30,000 years-old permafrost sample, and exhibits spherical virions of complex composition. In particular, we show that (i) assembly is initiated by a unique structure containing a flat pole positioned at the center of an open cisterna; (ii) core packing involves another cisterna-like element seemingly pushing core proteins into particles being assembled; (iii) specific filamentous structures contain the viral genome before packaging. Altogether, our findings increase our understanding on how complex giant viruses interact with their host and provide the foundation for future studies to elucidate the molecular mechanisms of Mollivirus assembly.

Introduction

Membrane dynamics is tightly controlled to perform cellular functions at specific locations. Fusion and fission reactions maintain organelle identity and integrity and ensure communication, protein secretion and degradation, lipid synthesis, uptake of nutrients, etc. (1, 2). As obligatory intracellular parasites, viruses hijack the host cell machinery and, in particular, target cellular membrane pathways for entry, *i.e.* fusion, endocytosis or phagocytosis (3), replication (4), assembly and egress (5-7).

Nucleocytoplasmic large DNA viruses (NCLDV) originally encompassed an extended viral group with members of the families *Poxviridae*, *Asfarviridae*, *Iridoviridae*, and *Phycodnaviridae* (8, 9), characterized by large particle and genome sizes. Replication of NCLDVs is either exclusively carried out in the cytoplasm of the host cell or is partially dependent on the nucleus for early gene-expression (10-17). NCLDVs form viral factories (VF) in infected cells, which are dedicated sites for viral transcription, replication and assembly, leading to a dramatic re-organization of the host cytoplasm (18-20). The presence of an inner membrane, surrounded and shaped by a viral capsid or scaffold protein, is also a common feature. The biogenesis and origin of this membrane has been the topic of intensive studies for Vaccinia virus (VACV), the type-species of the *Poxviridae* family. Our working model proposes that the assembling virion is composed of an open membrane sphere containing a single lipid bilayer shaped by a honeycomb-like scaffold. Open membrane intermediates, derived from the endoplasmic reticulum, contribute to the formation of the membrane sphere that closes once the DNA has been packed (21-26). Additional studies on African swine fever virus (27), Paramecium bursaria chlorella virus-1 (28), and Acanthamoeba polyphaga mimivirus (APMV) (29-32) also revealed the presence of open membrane intermediates and the formation of open membrane spheres shaped by the

assembly of a capsid on their convex side, suggesting a novel and common strategy for viral inner membrane assembly.

APMV was the first giant virus discovered and the founding member of a new family of DNA viruses characterized by viral particle dimensions in the micrometer range and genomes encoding up to 1,500 proteins: the *Mimiviridae* of the recently proposed "Megavirinae" (10, 33, 34). This rapidly expanding family appeared to be phylogenetically related to the other families of NCLDVs. However three recently proposed viral families, namely "Pandoraviridae" (35), "Pithoviridae" (36), and "Molliviridae" (37), share only a handful of genes and question the likeliness of a common origin for all giant viruses (38). Notably, their particles exhibit an internal membrane lining the virion internal capsid shell, even though particle morphotypes range from spherical or ovoid to amphora-shaped and are significantly different from the common icosahedral virions of APMV and most NCLDVs, with the exception of poxviruses (39, 40). The sole representative of the "Molliviridae", Mollivirus sibericum, recently isolated from a 30,000 years-old permafrost sample, displays spherical virions (~600 nm) with a thick coat or tegument covered with fibers (37). Here, we use a combination of 3D-EM techniques to provide a thorough characterization of membrane acquisition and virion assembly of the giant Mollivirus sibericum. Despite little homology with other large and giant viruses, our findings show that Mollivirus sibericum utilizes a strategy similar to NCLDVs for viral inner membrane assembly involving the recruitment and opening of cell-derived membrane intermediates. We also show that a cisterna with open curling ends and a central flat pole serves as a unique precursor for membrane assembly. The viral inner membrane is subsequently shaped by additional capsid layers assembled from the flat pole and DNA is packed prior to closure of particles on the spherical counterpoint of this pole. Collectively our analysis provides significant insights into the unique assembly of complex virions of the recently-isolated Mollivirus sibericum and suggests that viral inner

membrane assembly *via* open intermediates might be a common feature of several large and giant viruses infecting eukaryotes.

Results

Reorganization of the whole cell during infection and formation of a prominent viral factory

At 3 hours post-infection, viruses were found in large vacuoles, individually or in groups of 2 to 4 particles (Fig 1) as previously observed (37). Particles of Mollivirus sibericum like all other giant viruses characterized until now, are internalized by *Acanthamoeba castellanii* and undergo structural reorganization to fuse their inner membrane with the the surrounding vacuolar membrane (40). While the particle interior is completely substituted with cytoplasmic content (Fig 1), no electron dense core that could contain the viral genome was detected within the host cytoplasm as opposed to APMV and VACV but reminiscent of Pandoravirus and Pithovirus (40). At 8 hours post-infection, the host cell is completely rearranged with the formation of a prominent VF in the cytoplasm where viral replication and assembly of virions occur (Fig 2). In the majority of infected cells the nucleus appeared absent or greatly reorganized (Fig 2): loosing their spherical appearance, becoming smaller or characterized by mis-localized nucleoli at the nuclear periphery rather than in the center. VFs occupy the majority of the cellular space and contain virions at different stages of assembly and organelles such as mitochondria, endoplasmic reticulum and the Golgi complex are excluded towards the cell periphery, close to the plasma membrane (Fig 2) (20, 37, 41). Compared to uninfected cells (Movie S1), mitochondria in infected cells are smaller and elongated rather than spherical, having a shorter diameter (Table 1). The VFs appear less organized when compared to the assembly sites of APMV (13, 30, 31) and resemble more

VACV infected cells (20). The different stages of virus assembly, membrane precursors, viral crescents, and virions in the process of closure or maturation, were found within the VF without any specific arrangement (Fig 2 and 3). Inside the VFs, long filaments are observed (more visible in Fig 11 which are specific to Mollivirus sibericum infection and most likely of viral origin (37). They might be involved in genome replication and packaging but do not seem to participate in particle assembly *per se* (discussed below).

Membrane biogenesis guides the complex assembly of Mollivirus sibericum

Membrane precursors. The assembly of virions of Mollivirus sibericum is initiated by a unique membrane precursor, never reported for other NCLDVs (Fig 3b and enlargement in c-1 and c-3; indicated by a white star). This membrane precursor resembles a cisterna of unknown origin which is specifically associated with a flat pole in its center (Fig 4; indicated by a black braket) and displays open curling ends. In more mature particles with a thick electron-dense capsid layer, the flat pole appears as a membranous closed structure, appended on the convex side of the capsid, causing its flattening (Fig 5; indicated by a black braket). Based on the fact that the flat pole is present on the membrane precursor we identified and is located at the center of virions being assembled (Fig. 3b and c), we propose that capsid assembly (Fig 4 and 6) proceeds from this pole towards the open curling ends in a symmetrical manner.

Viral crescents. Typical crescent structures are formed upon elongation of the viral membrane precursor, shaped by a thick tegument or coat with at least two additional layers (Fig 3b and enlargement in c-2). The open inner membrane ends are uncoated and curl towards the exterior of the particles (Fig 6), similar to VACV-crescents (21). Large amounts of coated (74 ±7 nm in diameter) and uncoated vesicles (66 ±24.7 nm in diameter) are present at the

assembly sites that may actively participate in the assembly of the inner viral membrane (Fig 6 and 7). Uncoated vesicles of roughly 66 nm in diameter were reproducibly found in close proximity to the open ends of the growing vial particles (Table 2). In contrast to VACV, for which open vesicular intermediates are recruited to the assembly sites (21), the vesicles found in the vicinity of the growing virions of Mollivirus are closed. However, vesicles in contact with the membrane ends are opened, suggesting that rupture occurs upon contact with the growing viral membrane (Fig 6 and 7). We also observe a co-assembly phenomenon, already reported for VACV, where particles at different stages of assembly can be connected *via* their inner viral membrane (Fig 8). Packaging of the viral inner content is specifically associated with another cisterna-like element (Fig 3c-2; indicated by white arrowheads) and this structure is present on the opposite side of the flat pole (Fig 6; Table 2). The presence of ribosomes segregated on the side facing the cytoplasm suggests that it originates from the endoplasmic reticulum (Fig 9). Along the assembly process, the material found inside particles is densely packed and does not exhibit visible features. Interestingly, some material is already present at the concave side of the early crescents and becomes more obvious as the viral sphere expands (Fig 3c-1 and 2).

Closure of virions. At the end of assembly, closure of the inner membrane occurs on the opposite side of the initiation pole (Fig 3b and enlargement in c-3). At the site of closure, vesicles are often observed and might be involved in membrane sealing (Fig 10). With DNA-immunolabeling of thawed cryo-sections of infected cells, only particles that are mature or close-to-closure are labeled indicating that genome packaging occurs at the final stages of assembly, similar to VACV (40) and APMV (21, 26, 29, 30, 42). The immunolabeling is also detected on long filamentous structures (Fig 11) which are specific to Mollivirus sibericum infection and abundant in the VF. These DNA-associated filaments participate in DNA packaging and might therefore represent the viral nucleoproteins (Legendre et al., 2015) (Fig

12). Notably, the flat pole is present at all stages of assembly as well as on mature particles and is always located on the spherical counterpart compared to the sites used for membrane elongation and closure or DNA-uptake (Fig 12; indicated by a black braket).

Mature virions. Mature viruses are composed of at least one inner membrane enclosing dense material, two additional capsid layers and a thick tegument or coat covered with two layers of fibers (Fig 3b and enlargement in c-4; the different capsid layers are indicated and numbered). When observed from the top, on a tangential plane, the surface of the particle displays remarkable striations (Fig 3c-3 and 2c-4; indicated by white hashtag) as previously reported (37). One of the two additional capsid layers present in between the inner membrane and the tegument resembles a membrane when cells are embedded in resin (Fig 13, left panel; indicated by white arrows). However, only the inner structure appears white (Fig 3c-4 layer 3; Fig 13, right panel; indicated by white arrows) when using the Tokuyasu method, suggesting that there might be only one membrane in Mollivirus sibericum. Cryo-EM will be needed to solve virion structure at high resolution and under native conditions (43) in order to conclude.

Abundant membrane proteins in mollivirions

Using membrane prediction softwares (see Methods), we identified 27 proteins containing at least one transmembrane domain in the publicly available proteome of Mollivirus sibericum virions (37). Interestingly, structural and functional predictions of these membrane containing proteins highlight a remote homologue of the fusion protein of flaviviruses (ml_417); a lysosome-associated proteins (ml_309, ml_331) and vesicle-associated proteins (ml_448, ml_185); a possible cell adhesion protein (ml_499) and a homologue to a pore forming protein (ml_330) (Table 3), which in the context of our findings are interesting targets for future studies. The presence of these numerous membrane proteins composing about 20% of

the proteome of the purified viral particles (37), suggests that they could play an important role in the virion assembly process and in particular, in viral membrane acquisition including recruitment of cell-derived vesicles, fusion and rupture of membrane intermediates. Alternatively, they could also be involved in the initial fusion event necessary to initiate the infection, *i.e.* fusion of viral and cellular membranes prior to genome delivery. Furthermore, the major capsid protein (MCP, ml_347), only the 7th most abundant protein in the mature virions, might serve for scaffolding during virion assembly as observed for VACV (44). Interestingly, maturation of VACV virions includes proteolysis of the MCP, a prerequisite to the formation of non-icosahedral infectious virions. A similar process could also apply for Mollivirus sibericum and explain the changes in particle morphology observed upon exit of the mollivirions in the extracellular medium. The spherical neosynthesized virions become more flexible and elongated after being released from the host cells and undergo a dramatic change at the flat pole to form the large depression that will open and fuse with the vacuole membrane during the next round of infection (37). Such changes in terms of particle dimensions, shape and size of the flat pole, could be the result of proteolysis among other means and might correspond to the last stage of mollivirion maturation.

Discussion

Through the course of our study, protocols for sample preparation for 3D-EM analysis of *Acanthamoeba sp.*, infected or not, have been optimized and are now available. Our approach combines complementary EM techniques, *i.e.* FIB-SEM, ET and immunolabeling, to provide an in-depth characterization of the infection cycle of Mollivirus sibericum. We believe that our experimental design, which focuses mainly on 3D analysis of virion assembly, will serve as a basis for future studies on other giant and large DNA viruses in general.

We confirm previous findings on the internalization of the virions into vacuoles (37). Infection proceeds through the formation of a large cytoplasmic structure dedicated to genome replication and virus assembly, the viral factory (VF) (20, 37). In contrast to APMV, the VF appears to contain viruses at different stages of assembly with no specific arrangement similar to VACV (18-20). We used FIB-SEM to provide insights into the overall rearrangement of the cellular cytoplasm upon virus-infection (45). VFs occupy most of the cell interior pushing organelles towards the cell periphery and nuclei are also rarely observed at late stages of infection and may appear smaller with mis-localized nucleoli at the periphery. In general, infection with giant and large DNA viruses have different impact on the host nucleus such as persistence for members of the *Mimiviridae* (19, 31, 46), *Pithoviridae* (36) and *Poxviridae* (47), disruption, *e.g.* "Pandoraviridae" (35), or even transient recruitment of nuclear factors as recently reported for *Marseilleviridae* (48). In the case of Mollivirus sibericum, the viral genome is initially delivered into the nucleus and nuclear proteins are essential for early replication. At late stages, however, the function and fate of the nucleus remain ambiguous and it can either be maintained in some cells or completely destroyed in others. During infection, mitochondria become smaller and elongated when compared to control cells. Interestingly, it has been shown previously that several viruses, including poxviruses and asfarviruses, modulate mitochondrial metabolism towards fission and mitophagy to increase replication, attenuate apoptosis and promote viral persistence (49).

With both transmission EM and scanning transmission EM, we observed that virion assembly of Mollivirus sibericum relies on the general strategy of vesicle recruitment, opening and shaping by capsid layers similar to all NCLDVs studied up to now. However, membrane assembly in particular exhibits specific features: (i) assembly is initiated by a unique structure containing a flat pole positioned at the center of an open cisterna of unknown origin; (ii) the final packing of core proteins involves another cisterna-like element seemingly pushing core

material into the particle being assembled; (iii) using DNA immunolabeling, we also reveal the genomic nature of the filamentous structures unique to Mollivirus sibericum (Fig 14) (37). These DNA-associated filaments are abundant inside the VF; since virions are only labeled at the latest stages of assembly, we propose that DNA-uptake takes place at the very final stage, similar to VACV and APMV (26, 29, 30, 42). Finally, for all the studied NCLDVs the recruitment of open membrane intermediates in the VF was shown. For Mollivirus sibericum, however, the vesicles abundant in the VF were closed and seemingly opened only by contacting the curling ends of the growing viral membrane (27, 29, 30) suggesting that these membrane ends mediated their rupture.

The viral membrane is a key component of enveloped viruses and is necessary for cytoplasmic delivery of the viral core upon fusion. Cellular membrane modified by viruses may also serve as anchor for both non-structural and structural viral proteins, driving virion replication and assembly, respectively (50). Although NCLDVs and giant viruses exhibit different virion morphotypes and infect a wide range of hosts, they all contain an internal membrane. This internal membrane can work as a support for additional structural components, guiding the assembly process of virions and play a key role during disassembly to release the virion content including the viral genome into the cellular cytoplasm upon fusion. In light of our findings, we propose that the unconventional assembly of viral inner membrane is a shared feature of NCLDVs and giant viruses which involves the recruitment and opening of cell-derived vesicles. This general strategy could testify of a common origin, or rather be the sign of a convergent evolution.

In the case of VACV and African swine fever virus, collective data show that the viral membrane is derived from the endoplasmic reticulum (22, 27, 51, 52) and it has also been proposed that the other giant APMV assembles an inner viral membrane from vesicles originating from the endoplasmic reticulum (30). The origin of the membrane of Mollivirus

sibericum remains to be investigated. The lack of ribosomes on the cisterna initiator may suggest a role for the Golgi complex or the endoplasmic reticulum-Golgi interphase which is consistent with the extensive recruitment of coated vesicles in the VF. Membrane elongation *per se* is mediated by uncoated vesicles of unknown origin, whereas at the final stage of core packaging, we observed a role for a closed cisternal element containing segregated ribosomes that could also be derived from the endoplasmic reticulum.

Taken as a whole, our analysis improves our understanding of the replication cycle of the complex virions of Mollivirus sibericum and in particular, how it assembled in comparison with other virus-host systems. We could show that particles contain at least one inner membrane covered by a thick coat and two additional capsid layers with a specific pole. However, the detailed organization of the internal structure and packed material remains to be determined and future studies should aim at resolving the structure of virions at high resolution as previously done for APMV (32, 43, 53, 54). Notably, we also report on cisternae as unique precursors of the viral inner membrane with open curling ends triggering fusion and rupture of vesicles for elongation. The flat pole found at the center of the opened cisternae mediates assembly of additional capsid layers and remains visible on mature particles supporting an important role for virus entry and genome delivery as well. Such mechanism of membrane acquisition and virion assembly is, so far, unique to Mollivirus sibericum and appears as a new variation of the general strategy of recruitment and opening of cell-derived vesicles for the inner membrane assembly of NCLDVs (22, 29, 31).

Materials and Methods

Cell culture and virus infection

Conditions for cell culture and virus purification were as described previously (37). Briefly, *Acanthamoeba castellanii* (Douglas) Neff (ATCC 30010TM) were grown in PPYG medium, at 32°C and infected with Mollivirus sibericum at a multiplicity of infection of 10 particles/cell. Titration of particles was carried out with a Malassez counting chamber after staining with Toluidine blue.

Sample preparation for electron microscopy

Control and infected cells at 3 and 8 hours post-infection were chemically fixed in 2 steps. First, cells were incubated for 1h with 4% paraformaldehyde (EMS, USA) and 0.1% glutaraldehyde (Merck, Germany) in PHEM buffer (60 mM PIPES, 25 mM HEPES, 10 mM EGTA, and 4 mM $MgSO_4$, pH 6,9). Second, post-fixation was done overnight at 4°C with 2.5% glutaraldehyde in PHEM buffer.

Cells were washed with PHEM buffer, post-fixed for 1h with 1% OsO_4 (Merck, Germany) and 1.5% Potassium Ferracyanide (Merck, Germany), then incubated with 2% uranyl acetate (Merck, Germany) in H_2O for 1h and dehydrated in successive steps of 15 min in 25, 50, 75, 95 and 100% ethanol. The samples were subsequently infiltrated with Agar 100 epoxy resin (Agar Scientific, United Kingdom). Alternatively, cells were washed four times in PBS, incubated with 50 mM ammonium chloride for 10 min, pelleted (3,000g – 30 min) and re-suspended in a minimal amount of 20% BSA in PPYG. Cell pastes were transferred into a lecithin-coated sample holder type A (EMS, USA) and cryo-fixed with a high-pressure freezing machine (HPM 010; Bal-Tec Products, USA). Following cryo-fixation, the samples were freeze-substituted with 0.2% OsO_4, 0.1% uranyl acetate, 2% H_2O, and 4% methanol in acetone (EMS, USA) according to the following schedule: -90°C for 1h, 1.25°C/h for 8h, 3.8°C/h for 8h, 12.5°C/h for 4h and 0°C for 1h. The samples were rinsed four times in acetone and slowly infiltrated with Agar 100 epoxy resin.

After polymerization, samples were first processed on an Ultracut R microtome (Leica, Austria) to prepare 70 nm-thin sections that were collected on Formvar-coated copper grids (EMS, Washington, PA, USA) and post-stained with 4% uranyl acetate for 45 min and Reynold's lead citrate (Delta Microscopies, France) for 5 min. The grids were analyzed in a Tecnai T12 transmission electron microscope (Thermo Fisher Scientific, USA) operated at 120 kV and equipped with a Gatan BM Ultra scan (Gatan Inc., USA).

Focused-ion beam scanning electron microscopy

For focused-ion beam scanning electron microscopy, embedded samples after cryo-fixation and freeze-substitution were cut with an Ultra R microtome to obtain a flat surface. The sample was subsequently placed on a pin stub (Agar scientific, United Kingdom) and recovered with silver paint (Agar scientific, United Kingdom) except on the flat surface which was coated with a 20 nm-thick layer of gold/palladium in an Ion Beam Coater (Gatan Inc., USA) to avoid charge effect. The 3D imaging was done with a FIB-SEM Auriga (ZEISS, Germany). Another protective layer of platinum of 1 µm was deposited on the surface of the volume of interest using ion beam assisted deposition with 30 kV acceleration potential. The cross-section was milled using 10 nA ion beam current. The surface obtained was then polished using this time a 2 nA ion beam current. Sections during acquisition were made using a 500 µA ion beam current. SEM images were acquired at 10 nm pixel size for a picture size of 2048 with 2 keV acceleration voltage and an aperture of 30 µm with the back-scattered electron detector. Alignment of the acquired stack of images was done using ImageJ and all the segmentations and measurements with Amira 6.3 (Thermo Fisher Scientific, USA).

Electron tomography

For transmission electron tomography, embedded samples after cryo-fixation and freeze-substitution were cut into serial 200 nm-thick sections with an Ultracut R microtome and

collected on Formvar-coated copper parallel bar grids (EMS, USA). Protein A-gold particles of 15 nm (UMC-Utrecht, Netherlands) were applied on both sides of the sections and post-staining was performed as described above, if necessary. Dual-axis electron tomograms were collected on a F20 transmission electron microscope (Thermo Fisher Scientific, USA), operated at 200 kV and equipped with a Gatan US4000. Tomographic tilt ranges were collected using the SerialEM program (55), typically from -60° to +60° with an angular increment of 1°. For scanning transmission electron tomography, embedded samples were cut into serial 750 nm-thick sections and collected on Formvar-coated copper bar grids. Protein A-gold particles of 15 nm were applied on both sides of the sections and post-staining was performed as described above, if necessary. Single-axis tomograms were collected on a Jeol JEM-2100F operated at 200 kV and a bright field detector (Jeol, Japan) at a size of 1,024 x 1,024 pixels. Continuous tilt series were collected typically from -72° to 72° with an angular increment of 1.5°.

Images analysis

For ET, tilted images were aligned using gold fiducials as reference and WBP reconstruction was carried out in IMOD 4.9 software package. Manual segmentation, 3D surface rendering and videos were prepared with Amira 6.3. Measurements on FIB-SEM data were done on the segmented objects with the module “Label analysis” from Amira 6.3. For each object the following measurements were done: (1) Length, maximum of the Feret diameters; (2) Width, minimum of the Feret diameters; (3) Breadth, largest distance between two parallel lines touching the object without intersecting it and lying in a plane orthogonal to the maximum Feret diameter; (4) Thickness, the largest segment that touches the object by its end points and lying in a plane orthogonal to the maximum Feret diameter and orthogonal to the breadth diameter; (5) Sphericity, ratio between the Length and Breadth of an object with a ratio of 1 corresponding to a sphere.

Immunolabeling of thawed cryo-sections

Control and infected cells at 8 hours post-infection were chemically fixed with 4% paraformaldehyde and 0.1% glutaraldehyde in PHEM buffer for 1h and kept in 4% paraformaldehyde in PHEM until processed for Tokuyasu cryo-sectionning as previously described (56). In brief, thawed cryo-sections were blocked with 1% BSA in PBS, immunolabeled with anti-DNA antibody clone 3519 (abcam, United Kingdom) diluted to 1/1000 and 10 nm protein A-gold prior to contrasting with uranyl acetate in methylcellulose (1:9). Once dried, sections were observed on a Tecnai T12 transmission electron microscope operated at 120 kV and equipped with a Gatan BM Ultra scan. At least, three independent experiments were performed for each condition.

Virion proteins sequence analyses

Possible transmembrane segment were searched using the TMHMM V2.0 (http://www.cbs.dtu.dk/services/TMHMM/) (57) and Phobius (http://phobius.sbc.su.se/) servers (58). Functional and structural predictions were performed using the HHPRED server (https://toolkit.tuebingen.mpg.de/#/tools/hhpred) (59).

Acknowledgements

The Ultrastructural Bio-Imaging facility of the Institut Pasteur, Paris, directed by J. Krinjse-Locker is member of the national infrastructure France-BioImaging. We thank all the members of UBI and in particular, Martin Sachse for useful discussion, technical assistance and critical reading of the manuscript. We also want to thank Elsa Garcin for useful discussion about the manuscript and the figures.

References

1. **Schmick M, Bastiaens PIH.** 2014. The interdependence of membrane shape and cellular signal processing. Cell **156:**1132-1138.
2. **Harayama T, Riezman H.** 2018. Understanding the diversity of membrane lipid composition. Nat Rev Mol Cell Biol **19:**281-296.
3. **Yamauchi Y, Helenius A.** 2013. Virus entry at a glance. J Cell Sci **126:**1289-1295.
4. **Reid CR, Airo AM, Hobman TC.** 2015. The Virus-Host Interplay: Biogenesis of +RNA Replication Complexes. Viruses **7:**4385-4413.
5. **Rossman JS, Lamb RA.** 2011. Influenza virus assembly and budding. Virology **411:**229-236.
6. **Votteler J, Sundquist WI.** 2013. Virus budding and the ESCRT pathway. Cell Host Microbe **14:**232-241.
7. **Munz C.** 2017. Autophagy Proteins in Viral Exocytosis and Anti-Viral Immune Responses. Viruses **9**.
8. **Iyer LM, Aravind L, Koonin EV.** 2001. Common origin of four diverse families of large eukaryotic DNA viruses. J Virol **75:**11720-11734.
9. **Iyer LM, Balaji S, Koonin EV, Aravind L.** 2006. Evolutionary genomics of nucleo-cytoplasmic large DNA viruses. Virus Res **117:**156-184.
10. **Gallot-Lavallee L, Blanc G, Claverie JM.** 2017. Comparative Genomics of Chrysochromulina Ericina Virus and Other Microalga-Infecting Large DNA Viruses Highlights Their Intricate Evolutionary Relationship with the Established Mimiviridae Family. J Virol **91**.
11. **Arslan D, Legendre M, Seltzer V, Abergel C, Claverie JM.** 2011. Distant Mimivirus relative with a larger genome highlights the fundamental features of Megaviridae. Proc Natl Acad Sci U S A **108:**17486-17491.
12. **Legendre M, Audic S, Poirot O, Hingamp P, Seltzer V, Byrne D, Lartigue A, Lescot M, Bernadac A, Poulain J, Abergel C, Claverie JM.** 2010. mRNA deep sequencing reveals 75 new genes and a complex transcriptional landscape in Mimivirus. Genome Res **20:**664-674.
13. **Suzan-Monti M, La Scola B, Barrassi L, Espinosa L, Raoult D.** 2007. Ultrastructural characterization of the giant volcano-like virus factory of Acanthamoeba polyphaga Mimivirus. PLoS One **2:**e328.
14. **Renesto P, Abergel C, Decloquement P, Moinier D, Azza S, Ogata H, Fourquet P, Gorvel JP, Claverie JM.** 2006. Mimivirus giant particles incorporate a large fraction of anonymous and unique gene products. J Virol **80:**11678-11685.
15. **Rojo G, Garcia-Beato R, Vinuela E, Salas ML, Salas J.** 1999. Replication of African swine fever virus DNA in infected cells. Virology **257:**524-536.
16. **Van Etten JL, Burbank DE, Joshi J, Meints RH.** 1984. DNA synthesis in a Chlorella-like alga following infection with the virus PBCV-1. Virology **134:**443-449.
17. **Rohrmann G, Moss B.** 1985. Transcription of vaccinia virus early genes by a template-dependent soluble extract of purified virions. J Virol **56:**349-355.
18. **Risco C, de Castro IF, Sanz-Sanchez L, Narayan K, Grandinetti G, Subramaniam S.** 2014. Three-Dimensional Imaging of Viral Infections. Annu Rev Virol **1:**453-473.
19. **Mutsafi Y, Fridmann-Sirkis Y, Milrot E, Hevroni L, Minsky A.** 2014. Infection cycles of large DNA viruses: emerging themes and underlying questions. Virology **466-467:**3-14.
20. **de Castro IF, Volonte L, Risco C.** 2013. Virus factories: biogenesis and structural design. Cell Microbiol **15:**24-34.
21. **Chlanda P, Carbajal MA, Cyrklaff M, Griffiths G, Krijnse-Locker J.** 2009. Membrane rupture generates single open membrane sheets during vaccinia virus assembly. Cell Host Microbe **6:**81-90.
22. **Krijnse Locker J, Chlanda P, Sachsenheimer T, Brugger B.** 2013. Poxvirus membrane biogenesis: rupture not disruption. Cell Microbiol **15:**190-199.
23. **Moss B.** 2018. Origin of the poxviral membrane: A 50-year-old riddle. PLoS Pathog **14:**e1007002.
24. **Moss B.** 2015. Poxvirus membrane biogenesis. Virology **479-480:**619-626.

25. **Liu L, Cooper T, Howley PM, Hayball JD.** 2014. From crescent to mature virion: vaccinia virus assembly and maturation. Viruses **6:**3787-3808.
26. **Condit RC, Moussatche N, Traktman P.** 2006. In a nutshell: structure and assembly of the vaccinia virion. Adv Virus Res **66:**31-124.
27. **Suarez C, Andres G, Kolovou A, Hoppe S, Salas ML, Walther P, Krijnse Locker J.** 2015. African swine fever virus assembles a single membrane derived from rupture of the endoplasmic reticulum. Cell Microbiol **17:**1683-1698.
28. **Milrot E, Mutsafi Y, Fridmann-Sirkis Y, Shimoni E, Rechav K, Gurnon JR, Van Etten JL, Minsky A.** 2016. Virus-host interactions: insights from the replication cycle of the large Paramecium bursaria chlorella virus. Cell Microbiol **18:**3-16.
29. **Suarez C, Welsch S, Chlanda P, Hagen W, Hoppe S, Kolovou A, Pagnier I, Raoult D, Krijnse Locker J.** 2013. Open membranes are the precursors for assembly of large DNA viruses. Cell Microbiol **15:**1883-1895.
30. **Mutsafi Y, Shimoni E, Shimon A, Minsky A.** 2013. Membrane assembly during the infection cycle of the giant Mimivirus. PLoS Pathog **9:**e1003367.
31. **Mutsafi Y, Zauberman N, Sabanay I, Minsky A.** 2010. Vaccinia-like cytoplasmic replication of the giant Mimivirus. Proc Natl Acad Sci U S A **107:**5978-5982.
32. **Kuznetsov YG, Xiao C, Sun S, Raoult D, Rossmann M, McPherson A.** 2010. Atomic force microscopy investigation of the giant mimivirus. Virology **404:**127-137.
33. **Abrahao J, Silva L, Silva LS, Khalil JYB, Rodrigues R, Arantes T, Assis F, Boratto P, Andrade M, Kroon EG, Ribeiro B, Bergier I, Seligmann H, Ghigo E, Colson P, Levasseur A, Kroemer G, Raoult D, La Scola B.** 2018. Tailed giant Tupanvirus possesses the most complete translational apparatus of the known virosphere. Nat Commun **9:**749.
34. **Raoult D, Audic S, Robert C, Abergel C, Renesto P, Ogata H, La Scola B, Suzan M, Claverie JM.** 2004. The 1.2-megabase genome sequence of Mimivirus. Science **306:**1344-1350.
35. **Philippe N, Legendre M, Doutre G, Coute Y, Poirot O, Lescot M, Arslan D, Seltzer V, Bertaux L, Bruley C, Garin J, Claverie JM, Abergel C.** 2013. Pandoraviruses: amoeba viruses with genomes up to 2.5 Mb reaching that of parasitic eukaryotes. Science **341:**281-286.
36. **Legendre M, Bartoli J, Shmakova L, Jeudy S, Labadie K, Adrait A, Lescot M, Poirot O, Bertaux L, Bruley C, Coute Y, Rivkina E, Abergel C, Claverie JM.** 2014. Thirty-thousand-year-old distant relative of giant icosahedral DNA viruses with a pandoravirus morphology. Proc Natl Acad Sci U S A **111:**4274-4279.
37. **Legendre M, Lartigue A, Bertaux L, Jeudy S, Bartoli J, Lescot M, Alempic JM, Ramus C, Bruley C, Labadie K, Shmakova L, Rivkina E, Coute Y, Abergel C, Claverie JM.** 2015. In-depth study of Mollivirus sibericum, a new 30,000-y-old giant virus infecting Acanthamoeba. Proc Natl Acad Sci U S A **112:**E5327-5335.
38. **Koonin EV, Yutin N.** 2018. Multiple evolutionary origins of giant viruses. F1000Res **7**.
39. **Colson P, La Scola B, Levasseur A, Caetano-Anolles G, Raoult D.** 2017. Mimivirus: leading the way in the discovery of giant viruses of amoebae. Nat Rev Microbiol **15:**243-254.
40. **Abergel C, Legendre M, Claverie JM.** 2015. The rapidly expanding universe of giant viruses: Mimivirus, Pandoravirus, Pithovirus and Mollivirus. FEMS Microbiol Rev **39:**779-796.
41. **Miller S, Krijnse-Locker J.** 2008. Modification of intracellular membrane structures for virus replication. Nat Rev Microbiol **6:**363-374.
42. **Roberts KL, Smith GL.** 2008. Vaccinia virus morphogenesis and dissemination. Trends Microbiol **16:**472-479.
43. **Kaelber JT, Hryc CF, Chiu W.** 2017. Electron Cryomicroscopy of Viruses at Near-Atomic Resolutions. Annu Rev Virol **4:**287-308.
44. **Hyun JK, Accurso C, Hijnen M, Schult P, Pettikiriarachchi A, Mitra AK, Coulibaly F.** 2011. Membrane remodeling by the double-barrel scaffolding protein of poxvirus. PLoS Pathog **7:**e1002239.
45. **Narayan K, Subramaniam S.** 2015. Focused ion beams in biology. Nat Methods **12:**1021-1031.

46. **Claverie JM, Abergel C.** 2009. Mimivirus and its virophage. Annu Rev Genet **43:**49-66.
47. **Carter GC, Law M, Hollinshead M, Smith GL.** 2005. Entry of the vaccinia virus intracellular mature virion and its interactions with glycosaminoglycans. J Gen Virol **86:**1279-1290.
48. **Fabre E, Jeudy S, Santini S, Legendre M, Trauchessec M, Coute Y, Claverie JM, Abergel C.** 2017. Noumeavirus replication relies on a transient remote control of the host nucleus. Nat Commun **8:**15087.
49. **Khan M, Syed GH, Kim SJ, Siddiqui A.** 2015. Mitochondrial dynamics and viral infections: A close nexus. Biochim Biophys Acta **1853:**2822-2833.
50. **Perlmutter JD, Hagan MF.** 2015. Mechanisms of virus assembly. Annu Rev Phys Chem **66:**217-239.
51. **Weisberg AS, Maruri-Avidal L, Bisht H, Hansen BT, Schwartz CL, Fischer ER, Meng X, Xiang Y, Moss B.** 2017. Enigmatic origin of the poxvirus membrane from the endoplasmic reticulum shown by 3D imaging of vaccinia virus assembly mutants. Proc Natl Acad Sci U S A **114:**E11001-E11009.
52. **Sodeik B, Krijnse-Locker J.** 2002. Assembly of vaccinia virus revisited: de novo membrane synthesis or acquisition from the host? Trends Microbiol **10:**15-24.
53. **Xiao C, Rossmann MG.** 2011. Structures of giant icosahedral eukaryotic dsDNA viruses. Curr Opin Virol **1:**101-109.
54. **Ekeberg T, Svenda M, Abergel C, Maia FR, Seltzer V, Claverie JM, Hantke M, Jonsson O, Nettelblad C, van der Schot G, Liang M, DePonte DP, Barty A, Seibert MM, Iwan B, Andersson I, Loh ND, Martin AV, Chapman H, Bostedt C, Bozek JD, Ferguson KR, Krzywinski J, Epp SW, Rolles D, Rudenko A, Hartmann R, Kimmel N, Hajdu J.** 2015. Three-dimensional reconstruction of the giant mimivirus particle with an x-ray free-electron laser. Phys Rev Lett **114:**098102.
55. **Mastronarde DN.** 2005. Automated electron microscope tomography using robust prediction of specimen movements. J Struct Biol **152:**36-51.
56. **de Castro Martin IF, Fournier G, Sachse M, Pizarro-Cerda J, Risco C, Naffakh N.** 2017. Influenza virus genome reaches the plasma membrane via a modified endoplasmic reticulum and Rab11-dependent vesicles. Nat Commun **8:**1396.
57. **Krogh A, Larsson B, von Heijne G, Sonnhammer EL.** 2001. Predicting transmembrane protein topology with a hidden Markov model: application to complete genomes. J Mol Biol **305:**567-580.
58. **Kall L, Krogh A, Sonnhammer EL.** 2004. A combined transmembrane topology and signal peptide prediction method. J Mol Biol **338:**1027-1036.
59. **Zimmermann L, Stephens A, Nam SZ, Rau D, Kubler J, Lozajic M, Gabler F, Soding J, Lupas AN, Alva V.** 2018. A Completely Reimplemented MPI Bioinformatics Toolkit with a New HHpred Server at its Core. J Mol Biol **430:**2237-2243.

Figure legends

Fig 1. Transmission electron micrographs on the entry of Mollivirus sibericum. At 3 hours post-infection, cells of *Acanthamoeba castellanii* were fixed and processed for transmission electron microscopy after cryo-fixation and freeze-substitution. Entry of Mollivirus sibericum leads to (A) substitution of the viral inner content and (B-F) occurs via

endocytosis with multiple particles present in one vacuole with different shape and content; (G-I) individual particles with internal structures.

Fig 2. Analysis of whole-infected cells by focused-ion beam scanning electron microscopy. At 8 hours post-infection, cells of *Acanthamoeba castellanii* were fixed and processed for focused-ion beam scanning electron microscopy. (a) slice 535 through the reconstructed volume (acquired at 10x10x10 nm) with 3D surface rendering of infected cells. Scale bar, 2 µm. (b) slice 242 of the acquired volume and 3D surface rendering. (c) Projection with 3D surface rendering. (d) slice 592 through the reconstructed volume (acquired at 10x10x10 nm) with 3D surface rendering of infected cells. Scale bar, 1 µm. (e) slice 592 of the acquired volume and 3D surface rendering at different angles. The video of volume reconstruction with segmentation is shown in Supplementary Movie S2 (a-c) and Movie S3 (d-e). As indicated in the legend, mitochondria are segmented in yellow; endoplasmic reticulum in black; vesicles in green; empty virions in magenta; mature virions in dark blue; closure of virions in red; viral crescents in orange; and membrane precursors in cyan.

Fig 3. Observations of the different assembly stages of Mollivirus sibericum. At 8 hours post-infection, cells of *Acanthamoeba castellanii* were fixed and processed for scanning transmission electron tomography and transmission electron microscopy after cryo-fixation and freeze-substitution. (a) slice 40 through a tomogram acquired by scanning transmission electron tomography with underneath, projections of 3D surface rendering of particles being assembled. A detailed overview of slices through the tomogram including 3D surface rendering is shown in Figure 7. The video of the reconstructed volume with segmentation is shown in Supplementary Movie S4. The tegument is segmented in blue, additional capsid layers in dark green and the inner viral membrane in light green. Scale bar, 300 nm. (b) different stages of viral assembly can be observed by transmission electron microscopy: (1) curved membrane intermediates with open curling ends associated with a flat pole or covered

with the tegument and additional capsid layers; (2) typical open crescents associated with cisternae with segregated ribosomes; (3) closure of particles beginning with the inner viral membrane on the opposite side of the flat pole; (4) mature particles with thick tegument covered with fibers and encasing additional capsid layers, the inner viral membrane and dense material. Scale bar, 500 nm. (c) enlargements of the particles at different stages of assembly as depicted by black squares in (b). Membrane precursors are indicated by white stars in (1) and (3); the cisternae associated with viral crescents and segregated ribosomes, by white arrowheads; the flat pole is indicated by a black bracket (3) and the different capsid layers are numbered in (4). Note the top-views and tangential planes of particles in (3) and (4) which are indicated by a white hashtag and show the striations of capsids outer surface.

Fig 4. 3D-analysis of membrane precursor during assembly of Mollivirus sibericum particles. At 8 hours post-infection, cells of *Acanthamoeba castellanii* were fixed and processed for transmission electron tomography. (a) Slices 12 (left) and 94 (right) through the tomogram showing curved membrane intermediates with open curling ends associated with a flat pole and typical open crescents associated with cisternae. Scale bars, 200 nm. The flat pole is indicated by a black bracket. (b) projection images of 3D surface rendering of the particle showed in (a) with different angles. The video of volume reconstruction with segmentation is shown in Supplementary Movie S5. The tegument is segmented in blue; the additional capsid layers in dark green; the inner viral membrane in light green; and the flat pole in orange.

Fig 5. Transmission electron micrographs showing the flat pole on viral crescents. At 8 hours post-infection, cells of *Acanthamoeba castellanii* were fixed and processed for transmission electron microscopy after substitution at room temperature. Different stages of virus assembly are shown. The flat pole, indicated by a black bracket, is always visible at the opposite of the site where assembly proceeds. Scale bars, 200 nm (A, B) or 100 nm (C).

Fig 6. 3D-analysis of viral crescent during assembly of Mollivirus sibericum particles. At 8 hours post-infection, cells of *Acanthamoeba castellanii* were fixed and processed for transmission electron tomography. (a) Slices 16, 24 and 56 (from left to right) through the tomogram showing a typical viral crescent associated with a cisterna and displaying open curling ends. On the open curling end highlited with a black square, a vesicle comes into contact with the inner membrane and subsequently opens up. Scale bars, 200 nm. The flat pole is indicated by black bracket and one coated vesicle is labeled CV. (b) projection images of 3D surface rendering of the particle showed in (a) with different angles. The video of volume reconstruction with segmentation is shown in Supplementary Movie S5. The tegument is segmented in blue; the additional capsid layers in dark green; the inner viral membrane in light green; the flat pole in orange; and the cisternae in red.

Fig 7. Elongation of the viral inner membrane is triggered by binding to and opening of vesicles. At 8 hours post-infection, cells of *Acanthamoeba castellanii* were fixed and processed for transmission electron microscopy after cryo-fixation and freeze-substitution. Slices 20, 40, 60 and 80 (from top to bottom) through the tomogram are shown. The video of the reconstructed volume with segmentation is shown in Supplementary Movie S4. On the open curling end highlighted with a black square, a vesicle comes into contact with the inner membrane. Scale bars, 200 nm. The tegument is segmented in blue, additional capsid layers in dark green and the inner viral membrane in light green. On the open curling end of a viral crescent highlighted with a black square, a vesicle comes into contact with the inner membrane.

Fig 8. Co-assembly of multiple particles of Mollivirus sibericum. At 8 hours post-infection, cells of *Acanthamoeba castellanii* were fixed and processed for transmission electron tomography. (A) Slices 17 (left) and 80 (right) through the tomogram showing three particles being co-assembled including two connected through the inner viral membrane.

Scale bars, 200 nm. (B) projection images of 3D surface rendering of the particle showed in (A) with different angles. The video of volume reconstruction with segmentation is shown in Supplementary Movie S7. The tegument is segmented in blue, the additional capsid layers in dark green, the inner viral membrane in light green and the cisternae in red.

Fig 9. Viral crescents are associated with cisterna-like structures. At 8 hours post-infection, cells of *Acanthamoeba castellanii* were fixed and processed for transmission electron microscopy after cryo-fixation and freeze-substitution. Assembly of viral crescents is associated with cisterna-like structures which are seemingly pushing the viroplasm inside the particle being assembled. Scale bars, 250 nm. The cisternae are indicated with white arrowheads pointing to the side where the ribosomes are segregated.

Fig 10. 3D-analysis of closure of particles during assembly of Mollivirus sibericum particles. At 8 hours post-infection, cells of *Acanthamoeba castellanii* were fixed and processed for transmission electron tomography. (a) slices 53 (left) and 85 (right) through the tomogram showing closure of the inner membrane of particles. Scale bars, 200 nm. (b) projection images of 3D surface rendering of the particle showed in (a) with different angles. The video of volume reconstruction with segmentation is shown in Supplementary Movie S6. The tegument is segmented in blue; the additional capsid layers in dark green; the inner viral membrane in light green. Due to the orientation of the particle in the tomogram, the flat shaped pole is not visible and therefore not represented.

Fig 11. DNA-associated filaments involves in packaging during assembly of Mollivirus sibericum. At 8 hours post-infection, cells of *Acanthamoeba castellanii* were fixed and processed for immunolabeling of thawed cryo-sections. DNA-labeling is associated with viral filamentous structures and present in particles at the end of assembly. Scale bar, 500 nm.

Fig 12. DNA packaging occurs at the end of the assembly of Mollivirus sibericum. At 8 hours post-infection, cells of *Acanthamoeba castellanii* were fixed and processed for immunolabeling of thawed cryo-sections. DNA-labeling is: (A) absent from half-assembled particles and (B,C) observed inside mature and associated with viral filamentous structures. Scale bars, 200 nm (A) and 500 nm (B,C). The flat pole is indicated by black bracket.

Fig 13. Comparison of virions of Mollivirus sibericum prepared by classical embedding or Tokuyasu method. At 8 hours post-infection, cells of *Acanthamoeba castellanii* were processed for transmission electron microscopy after either cryo-fixation and freeze-substitution (left) or fixation and immunolabeling of thawed cryo-sections (right). Two of the inner capsid layers that appear like a membrane in resin-embedded samples (left) are indicated by white arrows and compared the corresponding structures in samples prepared by the Tokuyasu method (right). Scale bars, 200 nm (A) and 250 nm (B).

Fig 14. Schematic model of the assembly of Mollivirus sibericum. (1) Membrane assembly is initiated by an open cisternal element (light green) containing a flat pole (orange) at its center and core proteins (grey) are recruited at the opposite side of the membrane. (2) From this pole, additional protein layers: coat (light blue) and inner capsid layer (dark green) are recruited and shape the growing membrane into an open sphere or crescent. (3) The membrane grows by recruitment of vesicles that open upon contacting the open ends and final packaging of viral core proteins in crescents by a cisterna (red) located at the exact opposite of the flat pole; note that ribosomes are segregated on the side facing the cytoplasm. (4) Elongation of the membrane, packing of core proteins and recruitment of the tegument layer result in an almost completed particle with a remaining opening located at the opposite side of the flat pole, likely required to take up the viral genome (not shown). (5) Closure of the internal membrane with removal of material in excess.

Figure 1

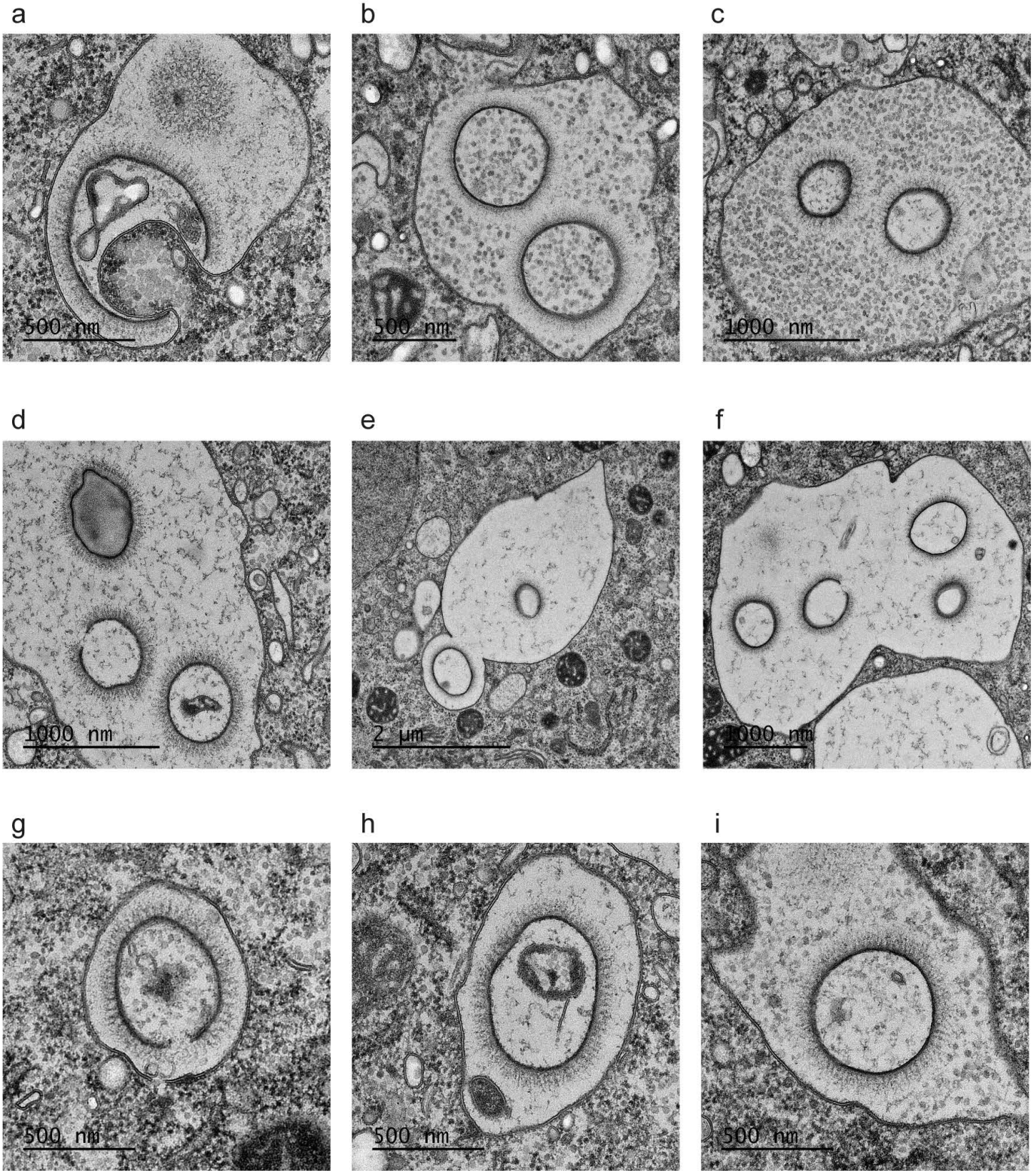
a
500 nm
b
500 nm
c
1000 nm
d
1000 nm
e
2 µm
f
1000 nm
g
500 nm
h
500 nm
i
500 nm

Figure 2

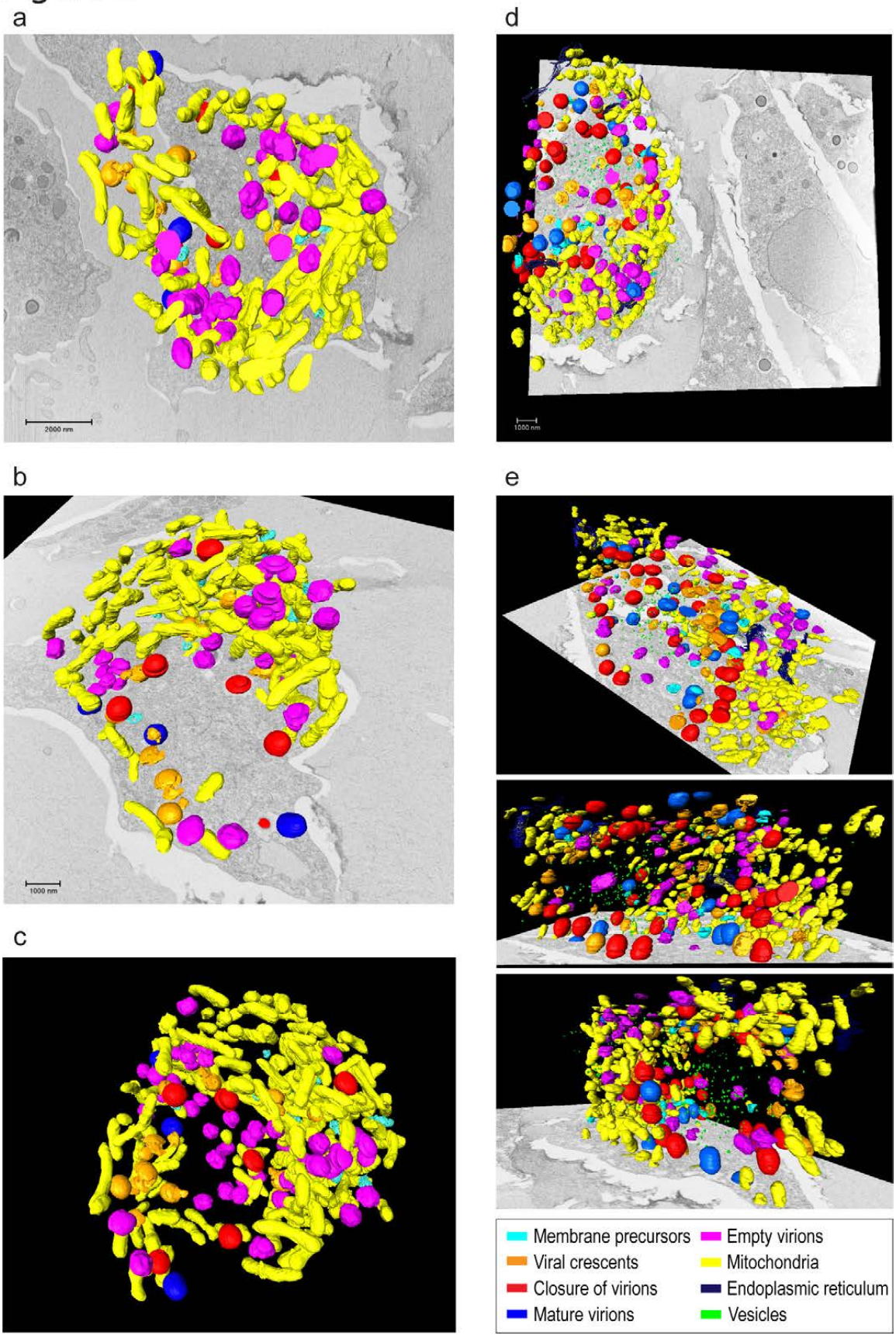
a
d
b
e
c
2000 nm
1000 nm
1000 nm
Membrane precursors
Empty virions
Viral crescents
Mitochondria
Closure of virions
Endoplasmic reticulum
Mature virions
Vesicles

Figure 3

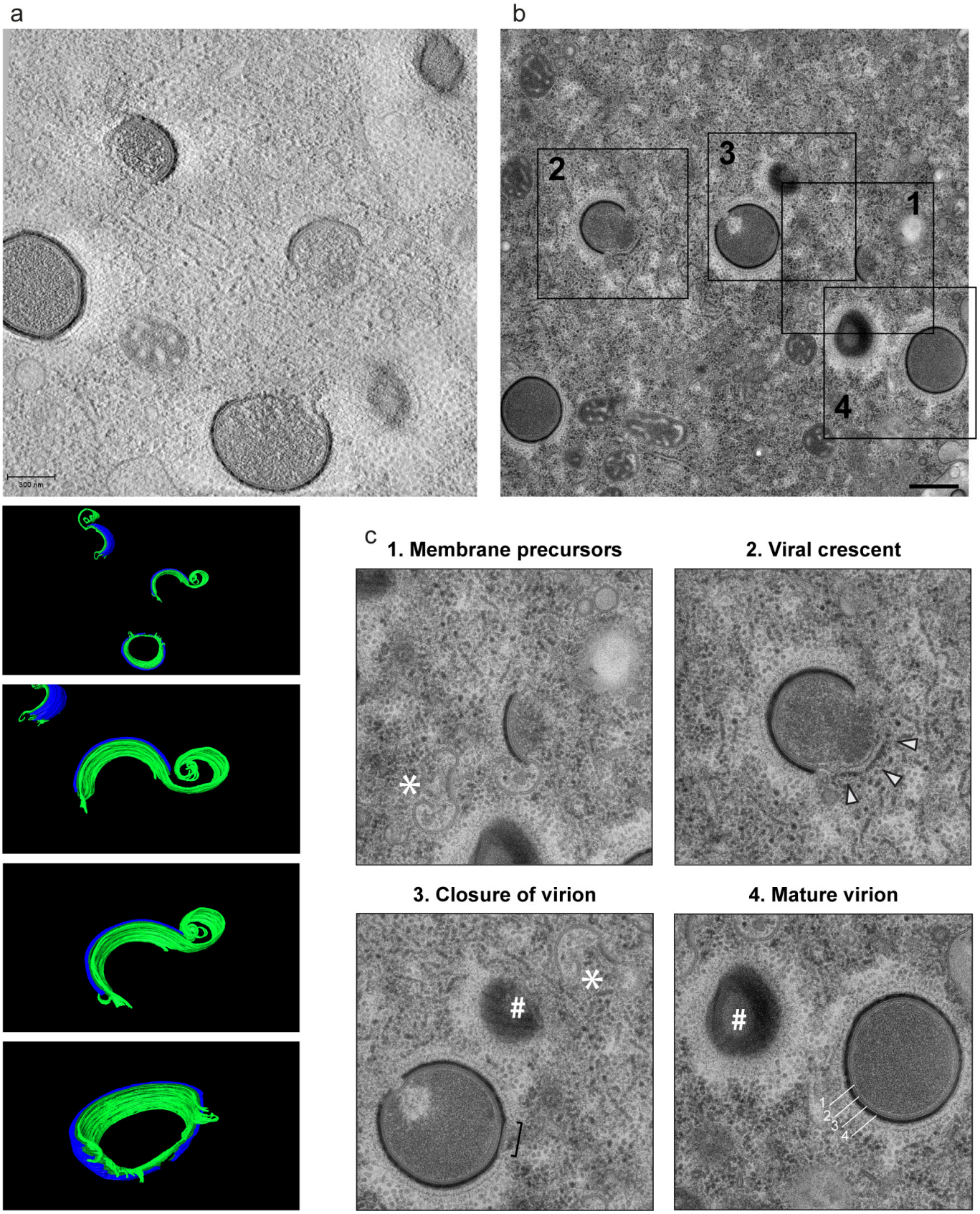
a
b
2
3
1
4
300 nm
c
1. Membrane precursors
2. Viral crescent
3. Closure of virion
4. Mature virion
1
2
3
4

Figure 4

a

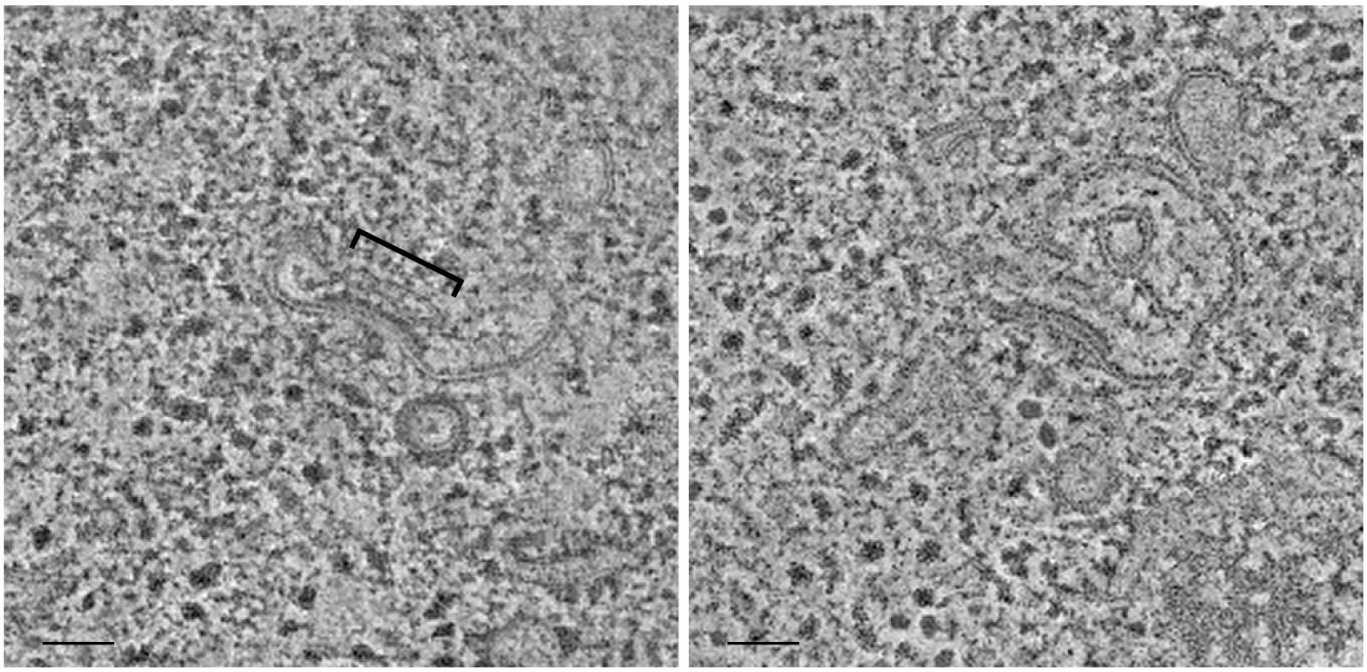

b

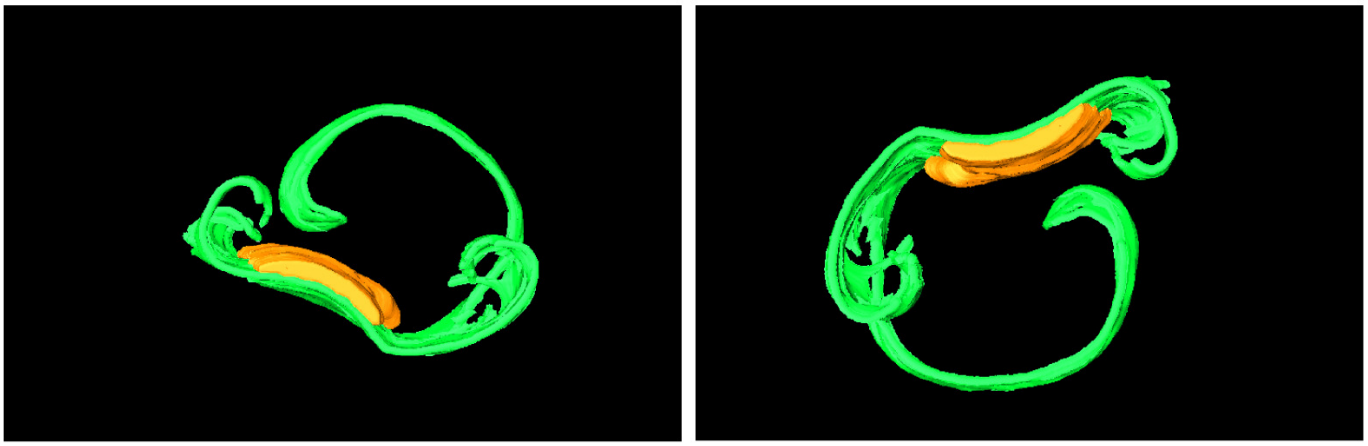

Figure 5

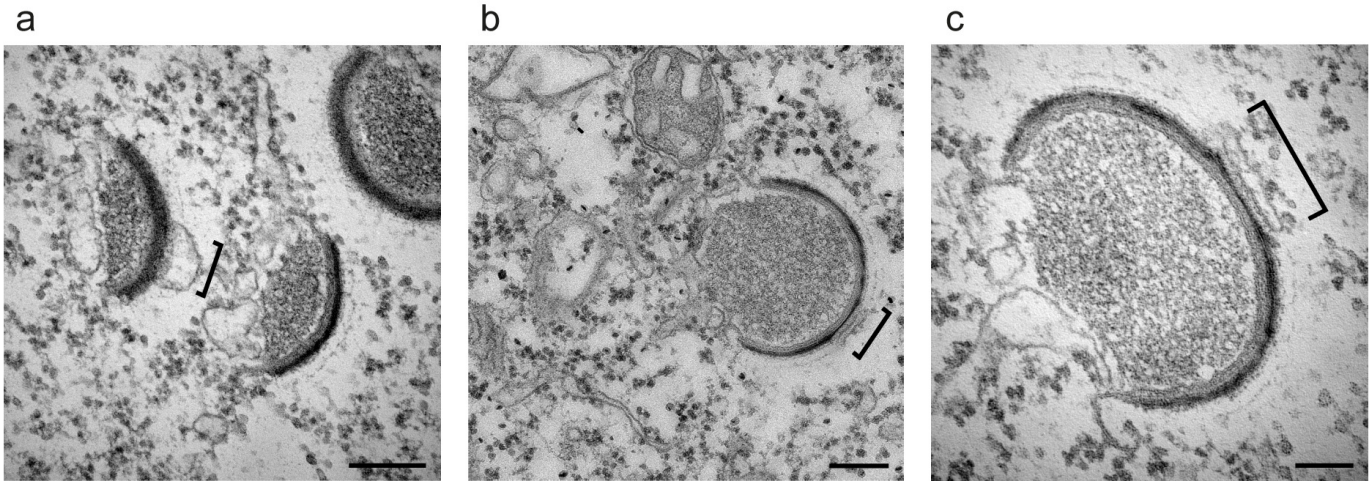

Figure 6

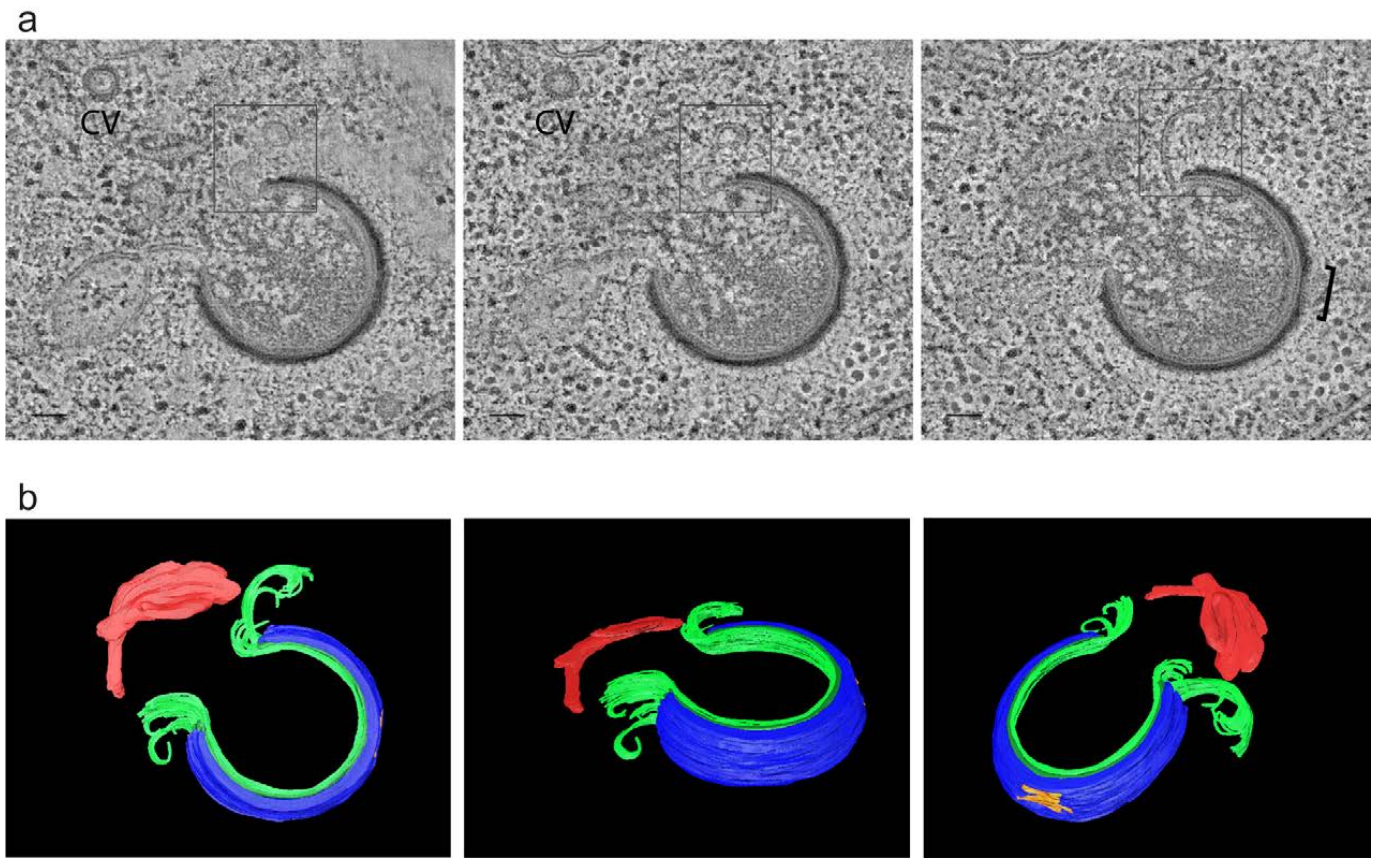

Figure 7

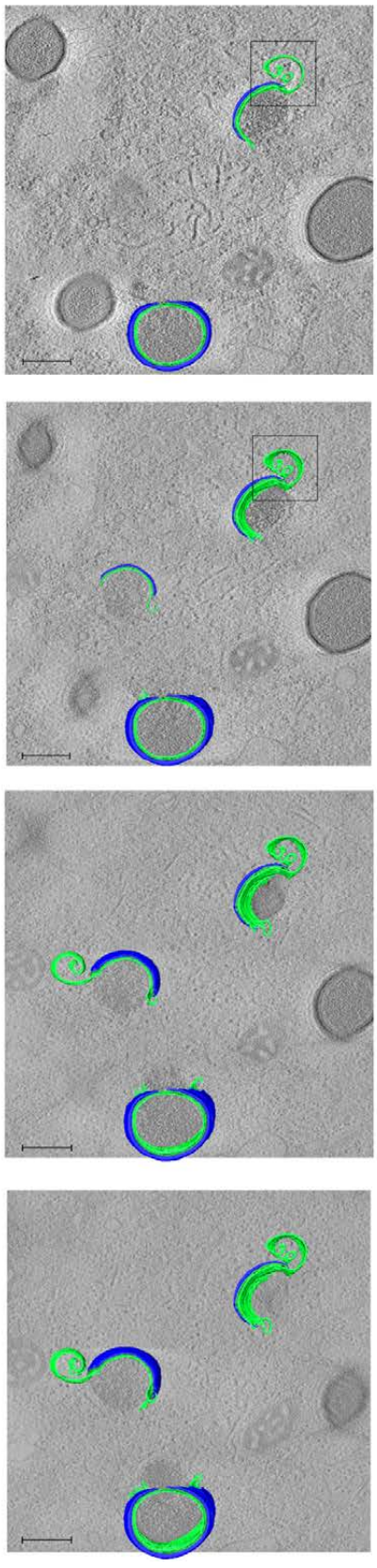

Figure 8

a

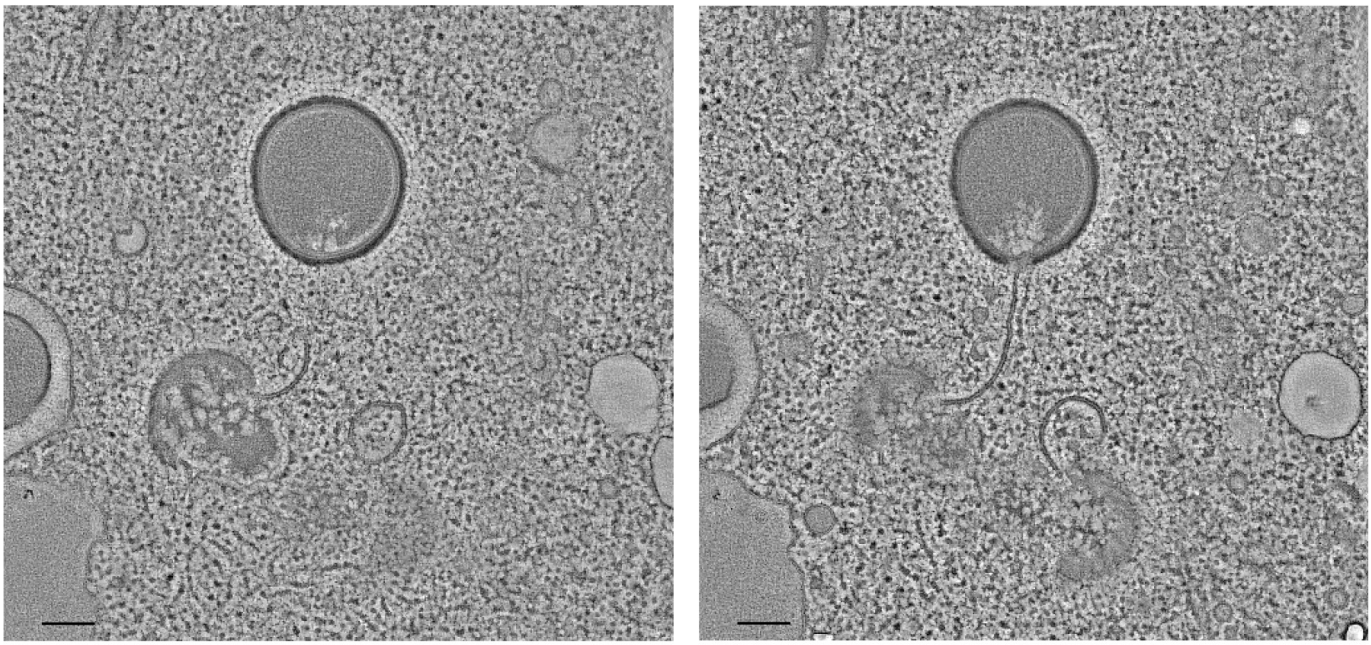

b

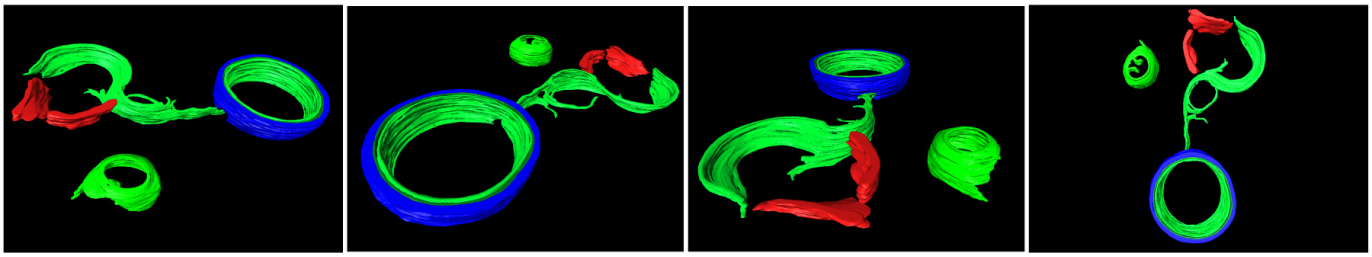

Figure 9

a

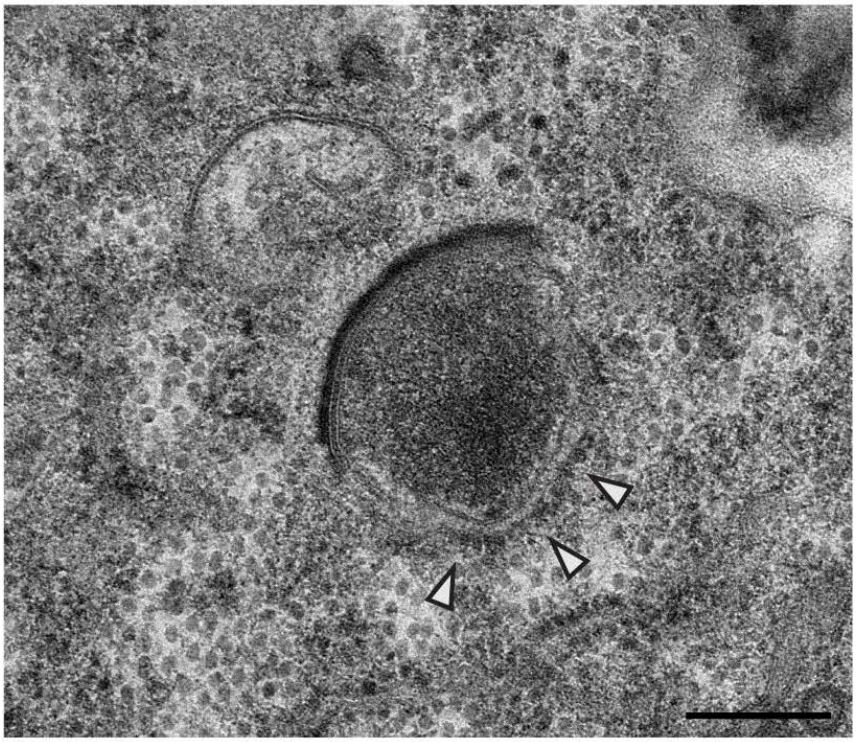

b

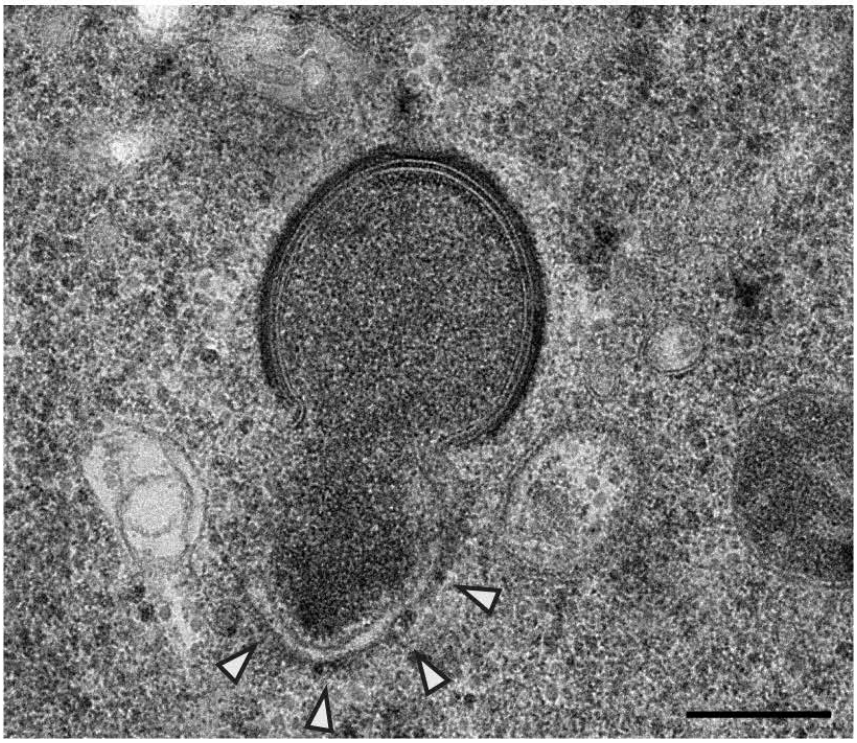

Figure 10

a

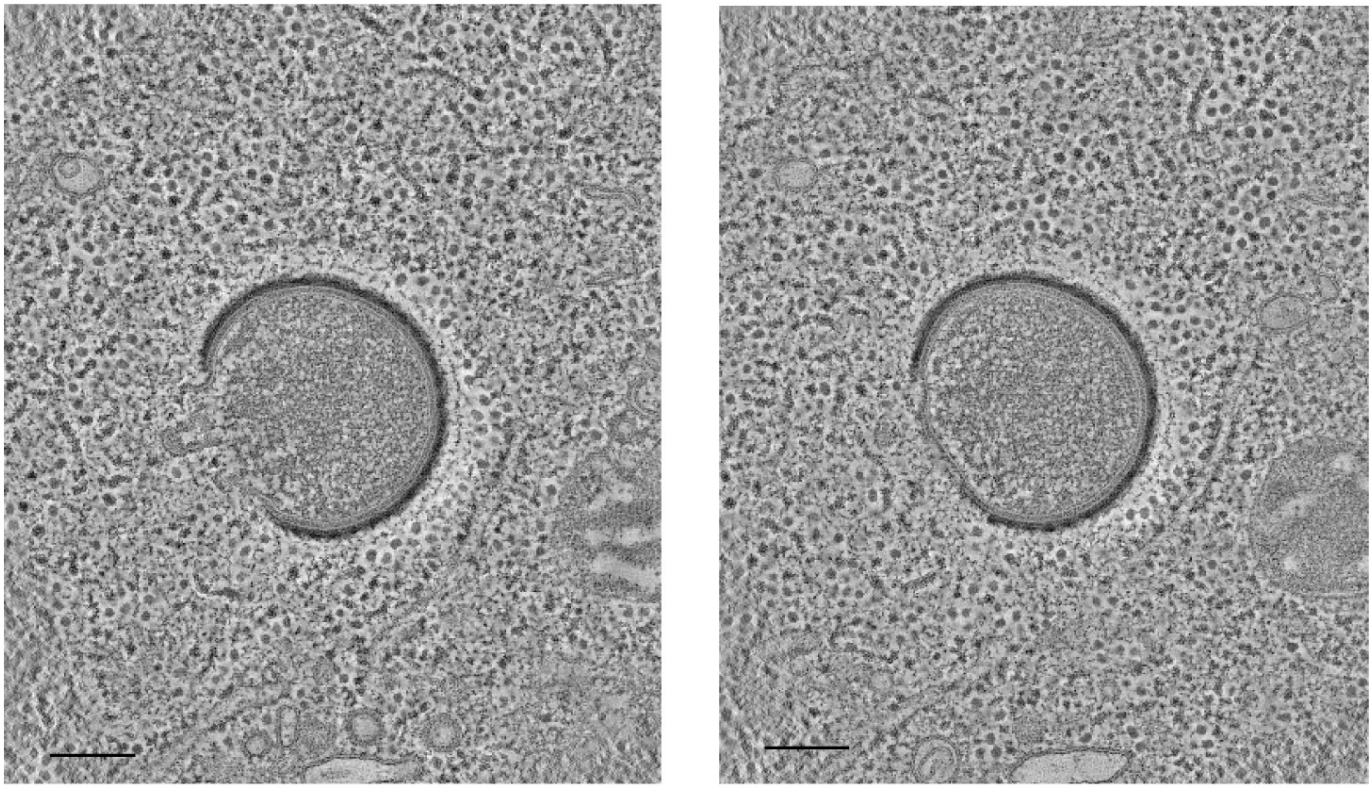

b

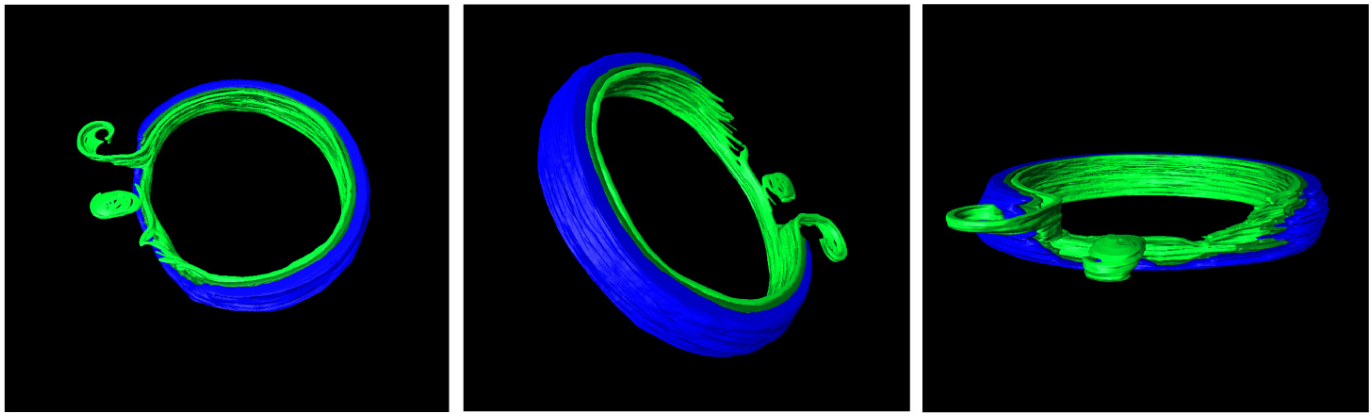

Figure 11

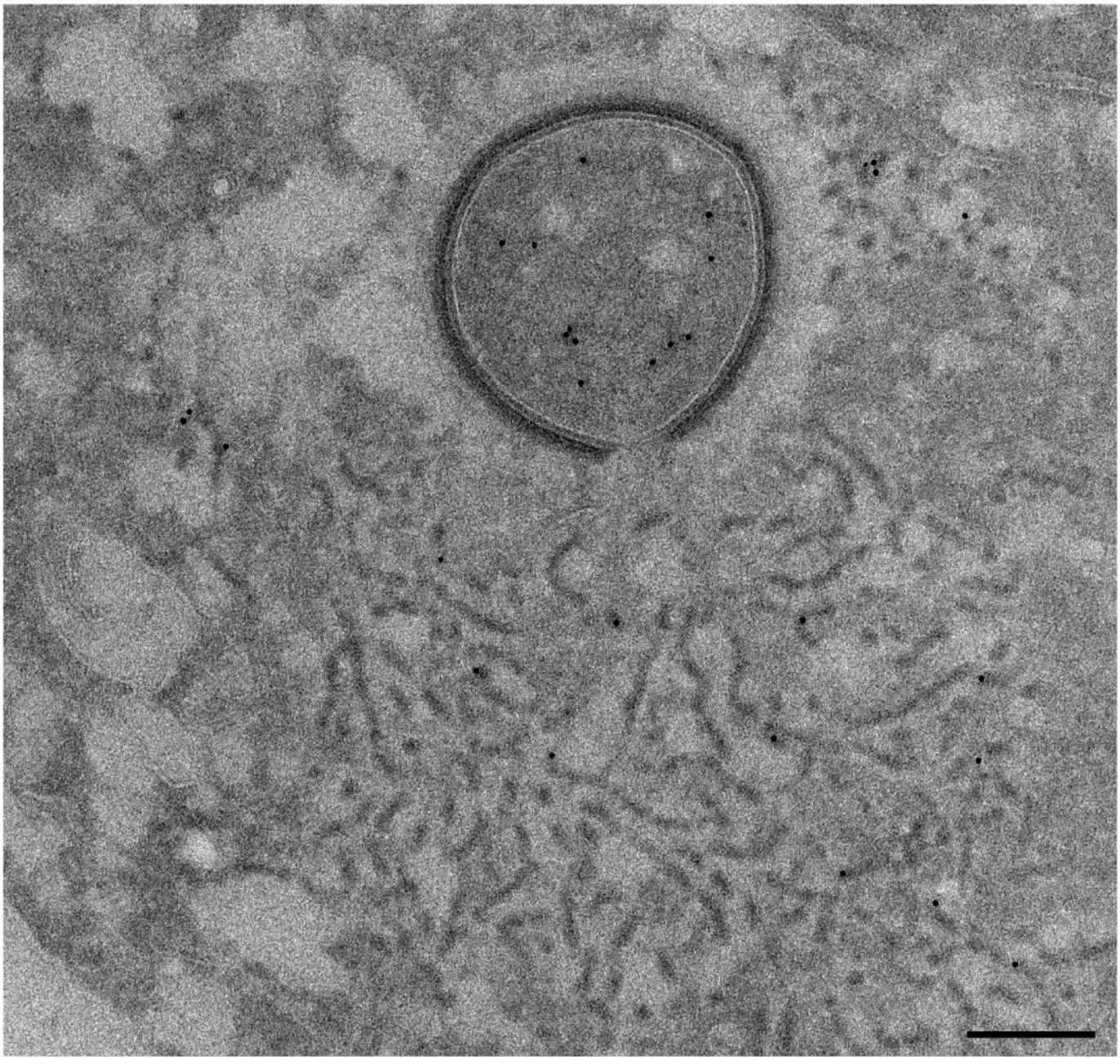

Figure 12

a

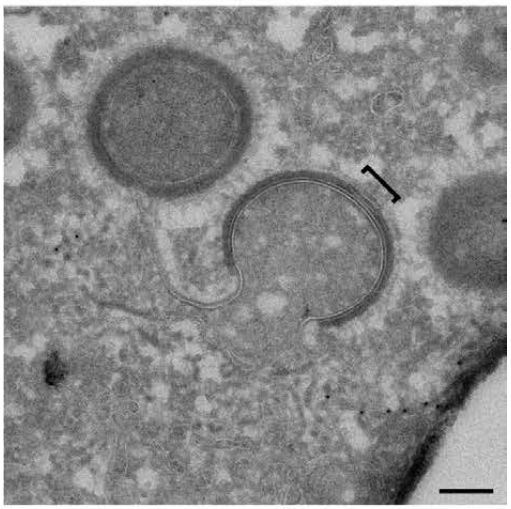

b

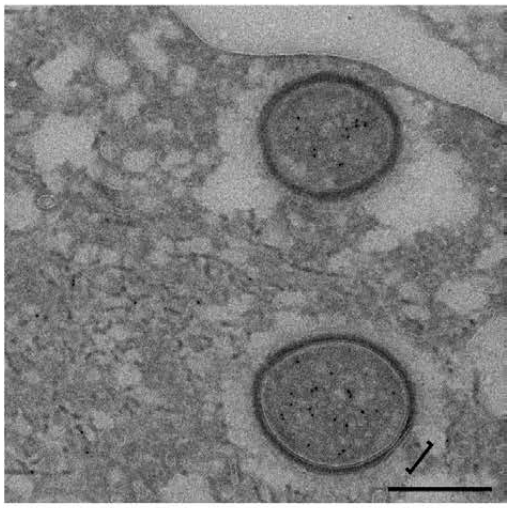

c

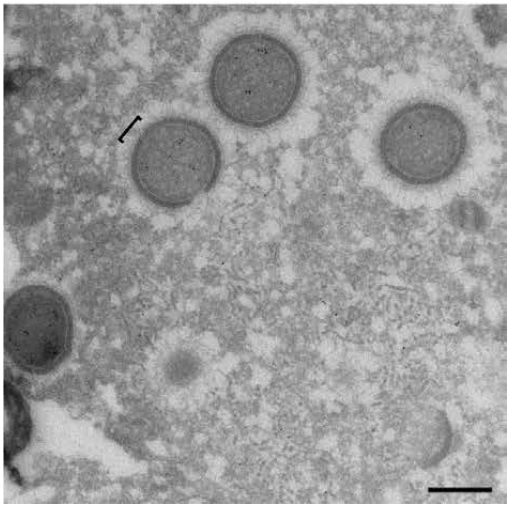

Figure 13

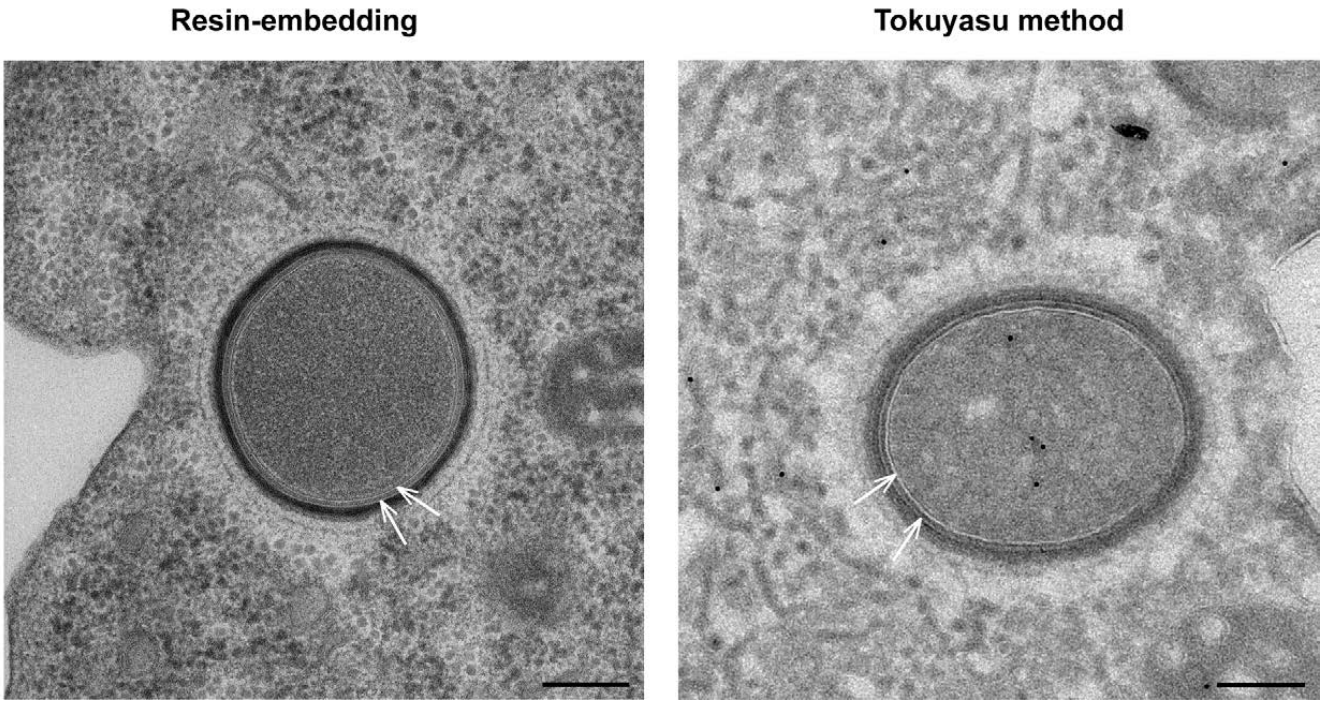

Figure 14

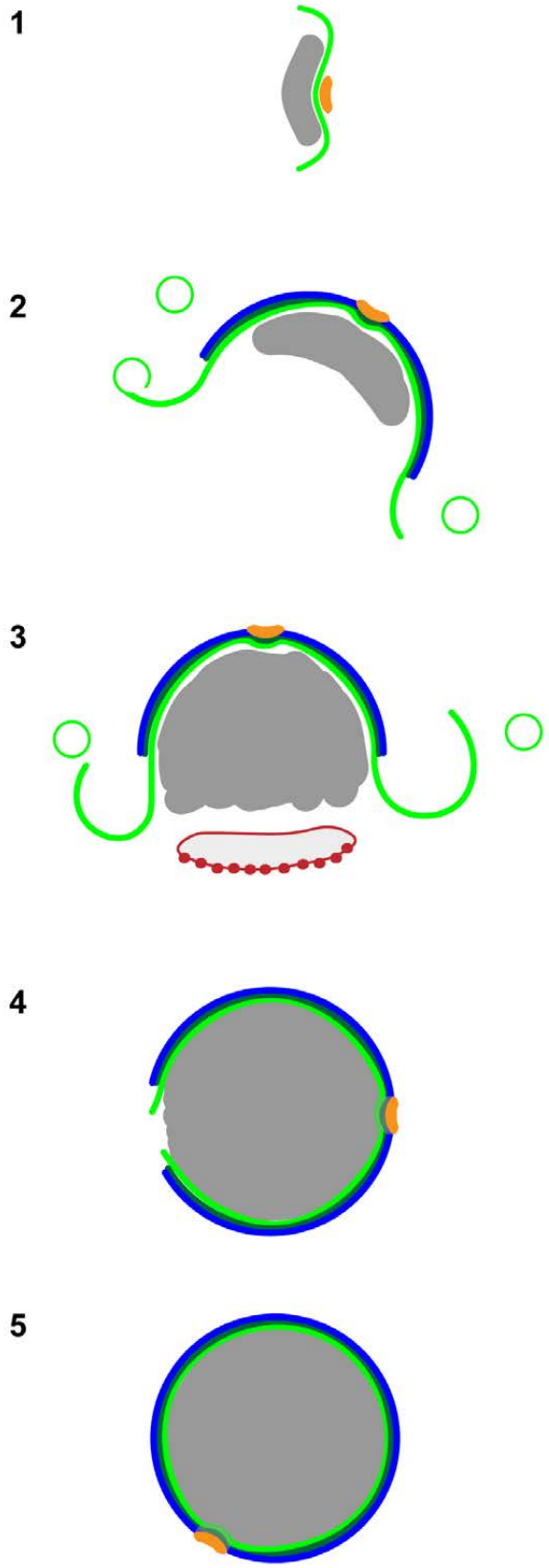

Table 1. Shape and dimensions of mitochondria in uninfected and infected cells.

Mitochondria	Length (nm)	Width (nm)	Breadth (nm)	Thickness (nm)	Volume (nm^3)	Sphericity
Uninfected cells	834.49 ±230.16	437.19 ±150.62	683.41 ±130.41	420.83 ±151.96	107 482 537.12 ±82 758 689.89	1.21 ±0.17
Infected cells	955.60 ±343.93	387.54 ±85.42	506.79 ±85.34	357.34 ±80.44	75 337 392.68 ±38 567 468.94	1.92 ±0.75

Table 1. Quantitative analysis of mitochondria observed in 3 uninfected (n=224) and 3 infected cells (n=596) acquired by focused-ion beam scanning electron microscopy: length, width, breadth, thickness, volume and sphericity. The average value and standard deviation are given for each condition (see Materials and Methods).

Table 2. Characteristics of virions observed by tomography at different stages of assembly.

Tomogram	Stage	End 1	End 2	Cisterna-like structure	Flat pole	Coated vesicles
1	Crescent	Open	Open	Present with ribosomes segregated	Observed	1
2	Crescent	Open	Open	Present with ribosomes segregated	Observed	2
3	Crescent	Open and connected to 2 vesicles	Open	Present with ribosomes segregated	Observed	0
4	Crescent	Open	Open	Present with ribosomes segregated	Observed	5
5	Crescent	Open	Open	Present with ribosomes segregated	Observed	5
6	Crescent	Open and connected to 2 vesicles	Open and connected to 2 vesicles	Present with ribosomes segregated	Observed	2
7	Crescent	Open and connected to 1 vesicle	Open	Present with ribosomes segregated	Not observed	0
8	Crescent	Open and connected to 3 vesicles	Open	Present with ribosomes segregated	Not observed	5
9	Crescent	Open and connected to 1 vesicle	Open	Present with ribosomes segregated	Not observed	10
10	Crescent	Open	Open	Present with ribosomes segregated	Not observed	5

11	Crescent	Open	Open	Present with ribosomes segregated	Not observed	0
12	Crescent	Open and connected to 1 vesicle	Open	Present with ribosomes segregated	Not observed	0
13	Crescent	Open	Open	Present with ribosomes segregated	Not observed	10
14	Crescent	Open and connected to 1 vesicle	Open	Present with ribosomes segregated	Not observed	10
15	Crescent	Open	Open	Present with ribosomes segregated	Not observed	5
16	Crescent	Open and connected to 1 vesicle	Open	Present with ribosomes segregated	Not observed	5
17	Closure of virions	-	-	Not observed	Not observed	1

Table 2. Characteristics of all virions imaged in 17 tomograms acquired through the course of our study are given depending on the stage of assembly of the virion. Crescents are defined as membrane structures that are composed of a membrane bended by the electron dense layer on its convex side, and exclude (almost) completed sphere. All viral crescents display two open ends that are sometimes found in close proximity and connected to vesicles; a cisterna-like structure is always associated with viral crescents but not with the one virion in the process of closure; and the flat pole is not always visible depending on the section plane. In the reconstructed volumes, coated vesicles are also often observed.

Table 3. List of hypothetical membrane proteins and major capsid protein in Mollivirus sibericum.

Protein number	Rank in Mollivirus proteome	Predictions, Transmembrane domain (TM)	Accession number
ml_436	3	1 TM	YP_009165402.1
ml_347	7	Major capsid protein related to NCLDVs	YP_009165313.1
ml_492	8	3 TM	YP_009165458.1
ml_222	9	1 TM	YP_009165188.1
mL_309	17	Lysosome-associated membrane glycoprotein, 1 TM	YP_009165275.1
ml_361	20	1 TM	YP_009165327.1
ml_499	21	Hydrolase, 1 TM	YP_009165465.1
ml_355	26	2 TM	YP_009165321.1
ml_331	33	Cell adhesion, 1 TM	YP_009165297.1
ml_330	34	Perforin-related protein related pleuroolysin, 1 TM	YP_009165296.1
ml_393	35	Antifreeze protein, 3 TM	YP_009165359.1
ml_285	37	Integrin, 1 TM	YP_009165251.1
ml_196	40	Hydrolase, 1 TM	YP_009165162.1
ml_367	41	ABC transporter, 1 TM	YP_009165333.1
ml_212	44	1 TM	YP_009165178.1
ml_402	49	1 TM	YP_009165368.1
ml_442	50	Receptor, 1 TM	YP_009165408.1
ml_417	53	Fusion protein, 2 TM	YP_009165383.1
ml_435	56	Sulfidryloxidase, 1 TM	YP_009165401.1

ml_353	65	Toxin, 1 TM	YP_009165319.1
ml_448	66	Vesicle-associated membrane protein, 2 TM	YP_009165414.1
mL_333	67	Channel protein, 1 TM	YP_009165299.1
ml_185	68	Vesicle associated protein, 1 TM	YP_009165151.1
ml_201	72	Carobxylesterase, 1 TM	YP_009165167.1
ml_399	78	Capsid protein related to poliovirus, 1 TM	YP_009165365.1
ml_321	94	1 TM	YP_009165287.1
ml_341	101	2 TM	YP_009165307.1
ml_307	104	Chemosensor, 2 TM	YP_009165273.1

Table 3. List of potential membrane proteins and major capsid protein in Mollivirus sibericum. Homologue to the major capsid protein of NCLDV containing hydrophobic segments and predicted transmembrane proteins identified in the proteome of Mollivirus sibericum are listed with protein number, rank in the proteome, predictions including number of transmembrane domains, and accession numbers. Possible transmembrane segment were searched using the TMHMM V2.0 and Phobius. Functional and structural predictions were performed using the HHPRED server.